JACS
JOURNAL OF THE AMERICAN CHEMICAL SOCIETY
Article
pubs.acs.org/JACS

Controlled Integration of Gold Nanoparticles and Organic Fluorophores Using Synthetically Modified MS2 Viral Capsids

Stacy L. Capehart,[†] Michael P. Coyle,[†,‡] Jeff E. Glasgow,[†] and Matthew B. Francis*[,†,‡]

[†]Department of Chemistry, University of California, Berkeley, California 94720-1460, United States
[‡]Materials Sciences Division, Lawrence Berkeley National Laboratories, Berkeley, California 94720-1460, United States

Supporting Information

ABSTRACT: The placement of fluorophores in close proximity to metal nanoparticle surfaces is proposed to enhance several photophysical properties of the dyes, potentially leading to improved quantum yields and decreased photobleaching. It is difficult in practice, however, to establish and maintain the nanoscale distances that are required to maximize these effects. The type of metal, size, and shape of the nanoparticle, the physical distance separating the metal nanoparticle from the organic dye, and the spectral properties of the fluorophore itself are all proposed to influence the quantum yield and lifetime. This results in a complex behavior that can lead to either enhanced or quenched fluorescence in different contexts. In this report, we describe a well-defined system that can be used to explore these effects, while physically preventing the fluorophores from contacting the nanoparticle surfaces. The basis of this system is the spherical protein capsid of bacteriophage MS2, which was used to house gold particles within its interior volume. The exterior surface of each capsid was then modified with Alexa Fluor 488 (AF 488) labeled DNA strands. By placing AF 488 dyes at distances of 3, 12, and 24 bp from the surface of capsids containing 10 nm gold nanoparticles, fluorescence intensity enhancements of 2.2, 1.2, and 1.0 were observed, respectively. A corresponding decrease in fluorescence lifetime was observed for each distance. Because of its well-defined and modular nature, this architecture allows the rapid exploration of the many variables involved in metal-controlled fluorescence, leading to a better understanding of this phenomenon.

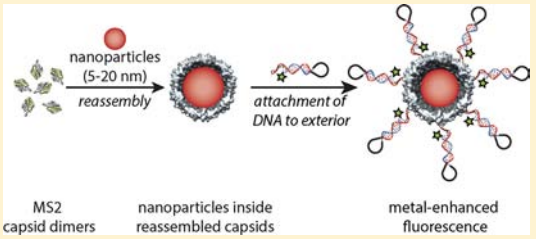

INTRODUCTION

Biological structures, such as proteins[1−6] and nucleic acids,[7−9] are finding increasing use for the positioning of multiple chemical groups into complex assemblies that have specifically defined orientations and spacings. These approaches capitalize on the nanoscale features inherent in biomolecules, which through self-assembly can bring attached components together into a functional whole. In addition to providing structural precision, modularity, and synthetic efficiency, the rigid nature of many biomolecules allows the distance relationships to be maintained after they are established. As ever more sophisticated targets are pursued, new bioconjugation methods will be required to allow different combinations of biomolecules to be merged with an expanding number of functional small molecules. In addition, methods will be required to interface biomolecules with inorganic surfaces and particles in a well-defined manner.

One compelling synthetic target for precise nanoscale synthesis is the controlled integration of organic dyes and metal nanoparticles, as this could allow the exploitation of an interesting phenomenon in nanophotonics.[10] It has been theoretically postulated and experimentally demonstrated that placing a metal nanoparticle in close proximity to an organic fluorophore significantly alters the photophysical properties of the fluorophore.[8,10−30] Through coupling interactions with the metal nanoparticle, the fluorophores are predicted to exhibit both an enhanced excitation rate and an accelerated radiative decay rate. This produces the desirable properties of an improved quantum yield and a decreased fluorescence lifetime, which could minimize competing photobleaching pathways.[14] Theoretical and experimental treatments have indicated that the type of metal, size and shape of the nanoparticle, the physical distance separating the metal surface from the organic dye, and the spectral properties of the fluorophore itself are all critical parameters for achieving a maximum effect.[8,10−30]

There are a number of experimental demonstrations of this behavior. As examples of a positive effect, a 2.5-fold increase in fluorescence emission has been observed for fluorophores deposited on copper nanoparticle films,[15] and an increase of up to 8-fold has been observed for organic dyes placed in close proximity (5 nm separation) to 80 nm gold nanoparticles.[26] In addition, an enhancement of 15-fold has been observed for dyes placed ∼7.5 nm from the surface of 50 nm silver nanoparticles.[20] In contrast, quenching of up to 99.8% has been observed for fluorophores placed 1−2 nm from a gold nanoparticle.[31]

Theoretical treatments[32] and experimental validations have shown quenching with a $1/R^4$ distance dependence for small (≤2 nm diameter) AuNPs[30,33,34] and enhancement for large

Received: August 7, 2012
Published: February 12, 2013

   dx.doi.org/10.1021/ja3078472 | J. Am. Chem. Soc. 2013, 135, 3011−3016

(>30 nm diameter) AuNPs.[26,35] However, many inconsistencies still exist in the literature as to the precise influence of AuNPs on organic dyes in the intermediate size regime. Some groups have reported fluorescence quenching near 5 and 10 nm diameter AuNPs.[8,29] Other groups have reported fluorescence enhancements between 2-fold and 17-fold for similarly sized AuNPs.[17,36,37]

These studies suggest that the interplay of the many involved variables results in an optimal metal−fluorophore distance that is platform-specific, making it difficult to probe these effects in a systematic manner. They also underscore the critical importance of physically separating the fluorophore from the particles to prevent direct contact quenching. This is a very difficult task in many cases, considering the nanoscale distances that are involved. What is needed to study these effects fully is a series of well-defined and readily adjusted architectures that can vary each of the independent parameters to modulate the fluorescence properties. To address this, we report herein a protein-based system that can establish desired metal−fluorophore distances, while simultaneously providing a physical barrier that prevents the dyes from coming into contact with the nanoparticle surfaces. We report the observation of gold nanoparticle-induced fluorescence enhancements, along with clear decreases in excited state lifetimes. Furthermore, these studies highlight the important role that covalently modified protein assemblies can play in the synthesis of multicomponent nanoscale materials.

RESULTS AND DISCUSSION

The biomolecular scaffold used to integrate the nanoparticles and chromophores in these studies was provided by the protein capsid of bacteriophage MS2.[38] This structure consists of a 27 nm diameter spherical hollow protein coat that self-assembles from 180 sequence identical monomers. The capsid remains intact upon exposure to a variety of conditions, including complete solvent removal, pH values from 3 to 10, and temperatures up to 55 °C (in H_2O).[39] Site-selective modification of MS2 has allowed for the incorporation of useful chemical functionalities on both the exterior and the interior surfaces of the capsid. Interior chemical modifications are normally made possible by the diffusion of small molecules through 2 nm pores in the protein shell—a strategy that had been used to attach taxol,[40] Gd-based MRI contrast agents,[41,42] ^{18}F PET labels,[43] and various small molecule fluorescent dyes[44,45] to amino acid residues on the inner surface. The exterior chemical modification of MS2 has involved the targeting of both native[46] and artificial[47] amino acids, and has been used to display peptides,[46−49] polymers,[46,48] and DNA aptamers[45] for use in biomedical applications. The external DNA strands have also been used to integrate the capsids into DNA origami assemblies.[50]

On the basis of the availability of the external modification strategy, we envisioned encapsulating a metal nanoparticle of interest on the interior of MS2 and using the external nucleic acid strands to place organic dyes at uniform fixed distances from the metal core (see scheme in Figure 2). The protein shell would prevent contact quenching between the metal nanoparticle and the exterior groups, and the sequence selectivity of DNA hybridization would allow a radially symmetric set of dyes to be located at desired distances. Several other groups have reported the encapsulation of metal nanoparticles by viral capsid proteins, allowing for the incorporation of quantum dots,[51] gold,[52−57] and cobalt iron oxide nanoparticles.[51,58] This suggests that several additional platforms could potentially be amenable to the strategy described herein, but none of these studies have combined the particle incorporation with synthetic modification of the capsid proteins.

In the case of MS2, other groups have reported the reassembly of MS2.[59,60] We recently reported a strategy to encapsulate DNA oligomers and negatively charged proteins by adding them to a pool of disassembled capsid proteins stabilized by trimethylammonium oxide as an osmolyte.[61] The reassembly presumably occurs as a result of electrostatic interactions between the anionic cargo and the building interior positive charge of forming capsids. In the current study, this methodology was also found to be applicable to encapsulation of DNA-coated gold nanoparticles (AuNPs). As outlined in Figure 1a, MS2 capsids were first disassembled in acetic acid and then reassembled in phosphate buffer in the presence of AuNPs labeled with ∼20−60 DNA strands (depending on the size of the AuNP). In the case of the AuNPs, the presence of

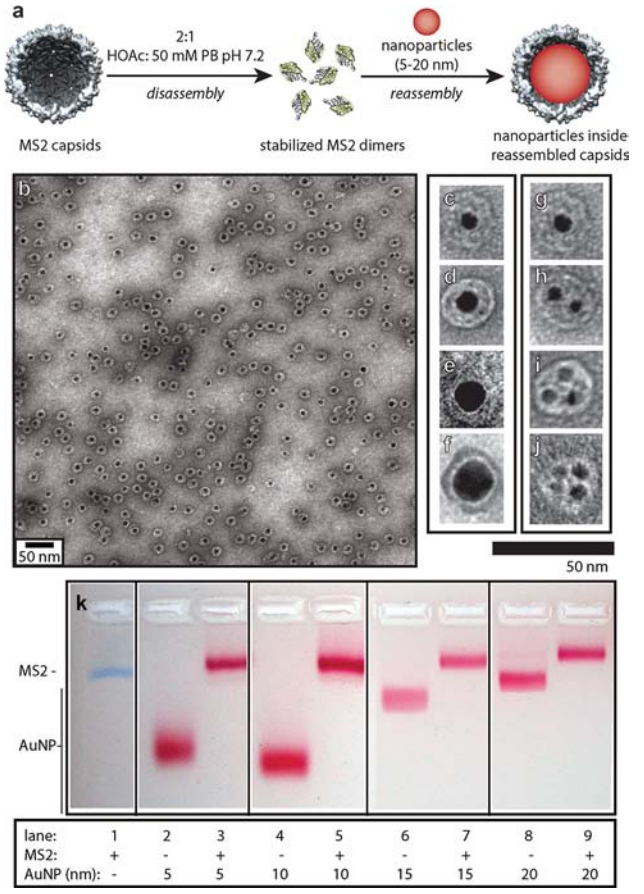

Figure 1. (a) T19*p*AF MS2 subjected to reassembly conditions in the presence of different sizes and concentrations of AuNPs. Transmission electron micrograph images of T19*p*AF MS2 reassembled around (b) 10 nm AuNPs, (c) 5 nm AuNPs, (d) 10 nm AuNPs, (e) 15 nm AuNPs, (f) 20 nm AuNPs, (g) one 5 nm AuNP, (h) two 5 nm AuNPs, (i) three 5 nm AuNPs, and (j) four 5 nm AuNPs. The native gel shown in (k) demonstrates similar electrophoretic mobility for MS2 reassembled around different size AuNPs (lanes 3, 5, 7, and 9) as particle-free MS2 (lane 1). The electrophoretic mobilities of the reassembled samples are different than their corresponding free AuNPs (lanes 2, 4, 6, and 8, respectively). Dynamic light scattering data and additional TEM images are reported in Supporting Information Figures S1 and S2.

dx.doi.org/10.1021/ja3078472 | J. Am. Chem. Soc. 2013, 135, 3011−3016

the osmolyte was not required, possibly due to the very high amount of negative charge on the metal surfaces. After 15−40 h of incubation at 4 °C, the capsids were observed to reform around 5, 10, 15, and 20 nm diameter AuNPs. In most cases, 60−90% of the capsids observed with transmission electron microscopy (TEM) contained nanoparticles (see specific numbers below). The presence of the AuNPs within the structures was confirmed through TEM (Figure 1b−j), and the encapsulated particles were found to run identically to native capsids using nondenaturing agarose gel electrophoresis (Figure 1k). Dynamic light scattering (DLS, Supporting Information Figure S1) showed minimal changes in the sizes of the assembled capsids for all four nanoparticle sizes. Interestingly, multiple particles could be captured inside some capsids when a large excess of 5 nm AuNPs was used (Figure 1h−j). The encapsulation of 40 nm particles, which are larger than the capsid interior, proved unsuccessful.

For our initial studies involving fluorophores, MS2 capsids containing 10 nm AuNPs were selected. As reported by another group using a similar viral capsid system, 10 nm AuNPs encapsulated most efficiently, resulting in the fewest unencapsulated AuNPs and empty viral capsids.[62] To install the exterior DNA strands, the assemblies were prepared using MS2 capsid proteins containing an unnatural amino acid, *p*-aminophenylalanine (*p*AF), introduced to position 19 using the amber stop codon suppression technique.[47,63] This provided 180 chemically distinct aniline groups on the outer surface, which we have previously targeted for modification using oxidative coupling reactions.[45,47,64] In this specific case, the distribution of reassembled T19*p*AF MS2 species around 10 nm AuNPs was characterized using TEM (see Supporting Information Figure S2). The majority of the assemblies consisted of capsids containing a single nanoparticle (77.2%), while capsids without AuNPs accounted for few of the observed structures (2.7%). Bare AuNPs (6.6%) and potentially misformed capsids (13.5%) comprised the remaining species. T19*p*AF MS2 successfully reassembled in the presence of 10 nm AuNPs modified with several different DNA sequences (Supporting Information Figure S3), suggesting that simple electrostatic interactions are sufficient to encourage reassembly. In addition, other MS2 mutants (T15Y N87C MS2 and T19Y N87C MS2) successfully reassembled in the presence of DNA modified 10 nm AuNPs, as confirmed by TEM, DLS, and native agarose gel electrophoresis (Supporting Information Figure S3). In the context of the experiments described below, these measurements suggest the critical parameter of diameter is identical for capsids with and without 10 nm AuNPs.

Samples of T19*p*AF MS2 capsids both with and without 10 nm DNA AuNPs were next modified to display external DNA strands. The *p*AF residues were exposed to 1 mM sodium periodate for 5 min in the prescence of 31, 38, and 54 nt hairpin strands bearing aminophenol groups at their 5′ termini and an AF 488 dye on their 3′ termini, as outlined in Figure 2.[45,48] Previous studies have shown that these conditions are compatible with the protein assembly and do not impair the hybridization ability of the DNA strands.[45] No effects were observed for the AuNPs as well, as judged by the retention of their surface plasmon band centered at 520 nm. The percent DNA modification of MS2 was quantified by SDS−PAGE gel electrophoresis using optical densitometry (Figure 3a), indicating similar modification levels for capsids with and without gold inside. Previous work exploring single silver nanoprisms indicated that maximum fluorescence enhancement

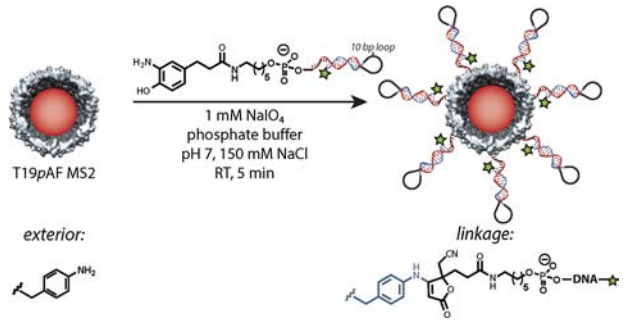

Figure 2. Overall synthetic strategy for constructing fluorophore−AuNP conjugates. For exterior surface modification, dye-labeled aminophenol-containing DNA can be attached to exterior anilines on T19*p*AF MS2 using a $NaIO_4$-mediated oxidative coupling reaction.

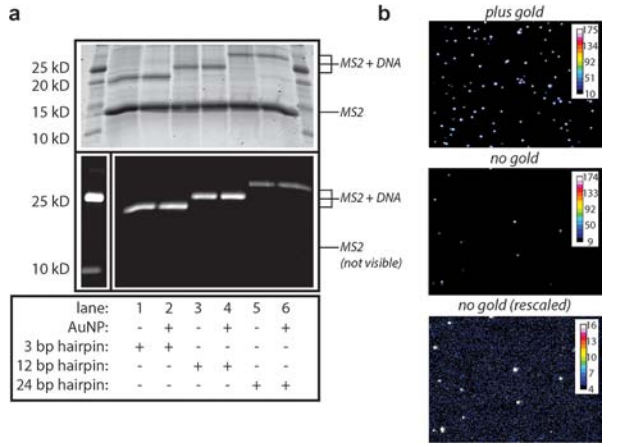

Figure 3. (a) MS2−DNA conjugates were analyzed by SDS−PAGE. Fluorescent bands were visualized under UV-light (bottom gel). Protein bands were visualized with exc. 532 nm and em. 610 nm following incubation with SYPRO ruby stain (top gel). The DNA modification was determined by optical densitometry to be ∼60 strands per capsid (33%), ∼45 strands per capsid (25%), and ∼34 strands (19%) for 3, 12, and 24 bp hairpin sequences, respectively. (b) MS2−DNA conjugates were visualized by TIRF microscopy for the 3 bp hairpin MS2 plus gold (top) and 3 bp hairpin MS2 minus gold (middle) case. The top and middle images are scaled the same. The bottom image was autoscaled. Larger versions of these images appear in Supporting Information Figure S4. The preparation of samples and glass slides for TIRF microscopy is described in Supporting Information text.

occurs with a dye that has a fluorescence emission slightly red-shifted from their surface plasmon band.[25] The emission spectrum of AF 488 directly overlaps with the surface plasmon resonance peak for 10 nm AuNPs, providing a close fit to this criterion. Excess fluorescently labeled DNA was removed through successive centrifugal filtrations with multiple 100 kDa molecular weight cutoff spin filters. DLS, nondenaturing agarose gel electrophoresis, and fluorescence correlation spectroscopy (FCS) were used to characterize the resulting constructs (Supporting Information Figures S8, S10, and S13). Each of these techniques suggested that the MS2 capsids were assembled, fluorescently labeled, and accompanied by few if any unattached fluorescently labeled DNA strands.

To explore the distance dependence of the enhancement, the synthetic procedure was used with different fluorophore−DNA sequences to position the dyes 3 bp from the capsid (1 nm from protein, 9.5 nm from the AuNP), 12 bp from the capsid

dx.doi.org/10.1021/ja3078472 | J. Am. Chem. Soc. 2013, 135, 3011−3016

(4 nm from the protein, 12.5 nm from the AuNP), and 24 bp from the capsid (8 nm from the protein, 16.5 nm from the AuNP). For the 12 and 24 bp distances, additional stabilizing strands were included to ensure that rigid double stranded DNA separated the fluorophores from the surfaces. Stabilizing strands were not included for the 3 bp distance.[65] A schematic for each of the six samples is shown in Figure 5b.

Total internal reflection fluorescence (TIRF) microscopy was used to measure the fluorescence intensity of the individual capsids in the six resulting samples (three distances with one set containing gold and another set without gold). The MS2–AuNP–fluorophore samples were incubated with glass slides bearing DNA strands that were complementary to those attached to the capsids, leading to the capture of the particles. The TIRF microscopy setup and surface modification is described in detail in the Supporting Information. Once a reasonable surface density was reached, a set of TIRF images was collected for each sample. Images for samples with and without gold particles are shown in Figure 3b, using identical scaling and acquisition parameters.

Each set of images was analyzed separately, and the results are shown in Figure 4. A distribution of intensities was

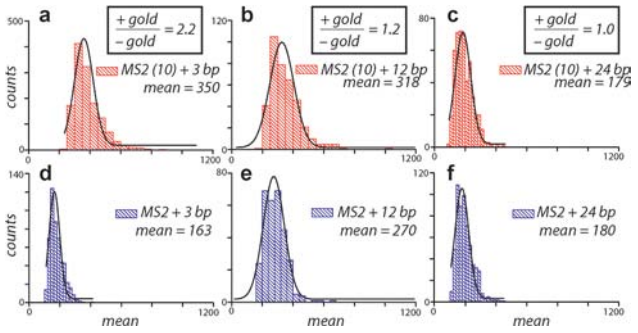

Figure 4. Mean intensity histograms determined from TIRF microscopy images for (a) 3 bp hairpin, (b) 12 bp hairpin, and (c) 24 bp hairpin MS2 capsids with gold as well as (d) 3 bp hairpin, (e) 12 bp hairpin, and (f) 24 bp hairpin MS2 capsids without gold samples. The black curves are Gaussian fits to the histogram data.

anticipated due to the differences in the levels of fluorescence labeling between individual capsids. The data are represented as mean intensity histograms, allowing the average brightness per particle to be compared in the presence and absence of gold particles.

The data plotted in Figure 4 are an exemplary data set, indicating a 2.2-fold enhancement for a 3 bp separation, a 1.2-fold enhancement for a 12 bp separation, and no effect was observed for a 24 bp separation when the gold particles were added to the capsids. Images were also collected using confocal microscopy. The confocal microscopy results agreed with the TIRF microscopy results and are shown in Supporting Information Figure S5.

Although one might anticipate the fluorophore brightness for each of the three gold-free samples to be identical, we attribute the observed changes in mean intensity among the gold-free samples to differences in fluorescence labeling. Higher modification levels may not necessarily result in increased sample brightness. Interactions between dyes attached to the capsid as well as interactions between the attached dyes and aromatic residues on the protein surface may affect the quantum yield of the fluorophore. Consequently, the most accurate comparisons are drawn only by comparing the samples with and without gold for each separation distance, as both samples have identical numbers of attached chromophores.

TIRF images were collected for multiple sample preparations, as well as a different MS2–DNA–fluorophore construct. Similar trends were observed throughout these sample sets. The results are detailed in the Supporting Information.

Fluorescence lifetime data were also collected for the AF 488 dye, three analogous DNA constructs, three MS2 samples without AuNPs, and three MS2 samples with AuNPs. A representative fluorescence lifetime trace overlaid with the instrument response function is plotted in Figure 5a. A decrease

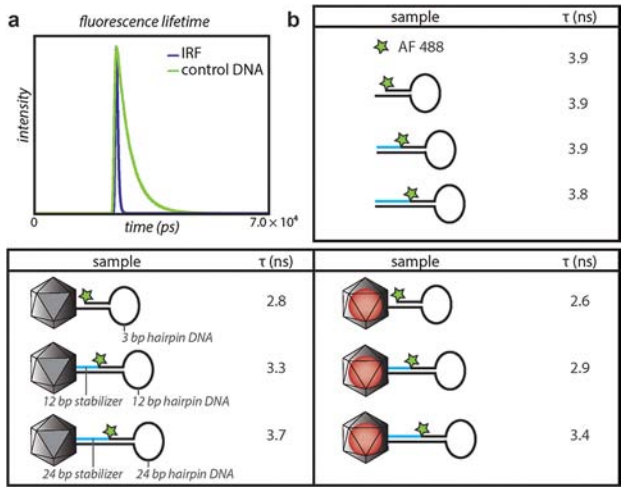

Figure 5. Fluorescence lifetime analysis of MS2-DNA conjugates. (a) Representative fluorescence lifetime trace of a control AF 488 DNA sample (green curve) overlaid with the instrument response function (IRF, blue curve). (b) Fluorescence lifetime data are tabulated for free AF 488, three DNA control samples, as well as three MS2 distances with and without gold. Error on lifetime measurements is determined to be approximately 0.1 ns.

in fluorescence lifetime was observed when the fluorophores were placed close to the gold-free capsid surface, with the shortest lifetime observed for the smallest separation between the fluorophore and protein, as tabulated in Figure 5b. We attribute this decrease in lifetime to interactions between the AF 488 and either other dyes attached to the capsid or aromatic residues on the capsid. A further decrease in fluorescence lifetime was observed for each of the samples with AuNPs on the interior surface, with the shortest lifetime at the smallest separation. This decrease in lifetime was in accordance with other groups that have reported fluorescence enhancement.[15,18−21,23,24] This effect is likely due to an increased radiative decay rate as a result of the AuNP being in close proximity to the fluorophores.

A control lifetime experiment was conducted with 10 nm AuNPs that were modified with multiple DNA strands, and then incubated with complementary fluorescently labeled DNA strands. These designs placed fluorophores 9.5, 12.5, and 16.5 nm from the AuNP surface. We were not able to obtain reasonable fits of fluorescence lifetimes for these data at concentrations similar to those used for capsid samples, due to low photon counts. This suggests the dyes are able to directly contact the surface of the AuNP, quenching their fluorescence. These results have been described in bulk fluorescence measurements for a similar system.[66] This is in sharp contrast

to the results we see where the metal nanoparticle is encapsulated in the viral capsid.

CONCLUSIONS

These studies demonstrate the utility of nanoscale protein assemblies for the integration of multiple components into complex systems. The precise dimensions of the viral capsids, in addition to the distinct chemically addressable exterior and interior surfaces, were crucially important for positioning of the dyes without allowing metal surface contact. In ongoing studies, we are using this synthetic system to explore an expanded range of metals, nanocrystal sizes, and fluorophore spectral properties. We are also exploring the use of additional protein scaffolds for the construction of fluorophore−nanoparticle structures with different geometric relationships. In addition to providing experimental tests of metal-enhanced fluorescence, the availability of these systems will provide valuable synthetic routes to access these structures for use in future applications.

ASSOCIATED CONTENT

Supporting Information

Supplementary experiments, full experimental details, dynamic light scattering traces, and transmission electron microscopy images. This material is available free of charge via the Internet at http://pubs.acs.org.

AUTHOR INFORMATION

Corresponding Author

mbfrancis@berkeley.edu

Notes

The authors declare no competing financial interest.

ACKNOWLEDGMENTS

These studies were generously supported by the Director, Office of Science, Materials Sciences and Engineering Division, of the U.S. Department of Energy under Contract No. DE-AC02-05CH11231. S.L.C. was supported by an NSF graduate research fellowship (2010101391). The U.C. Berkeley Chemical Biology Graduate Program (NIH Training Grant 1 T32 GMO66698) is acknowledged for the support of M.P.C. and J.E.G. Benjamin W. Caplins provided assistance with lifetime fitting, Allie C. Obermeyer synthesized the *o*-nitrophenol NHS ester used for amine DNA modification, Sune M. Christensen assisted with the preparation of glass coverslips, and Kristen L. Seim produced the T15Y N87C MS2 and T19Y N87C MS2 mutants discussed in the Supporting Information text. The laboratory of Peter G. Schultz is gratefully acknowledged for providing the plasmids required to introduce *p*AF into the capsids using the amber codon suppression technique.

REFERENCES

(1) Douglas, T.; Young, M. *Nature* **1998**, *393*, 152−155.
(2) Fiedler, J. D.; Brown, S. D.; Lau, J. L.; Finn, M. G. *Angew. Chem., Int. Ed.* **2010**, *49*, 9648−9651.
(3) Stephanopoulos, N.; Carrico, Z. M.; Francis, M. B. *Angew. Chem., Int. Ed.* **2009**, *48*, 9498−9502.
(4) Nam, Y. S.; Shin, T.; Park, H.; Magyar, A. P.; Choi, K.; Fantner, G.; Nelson, K. A.; Belcher, A. M. *J. Am. Chem. Soc.* **2010**, *132*, 1462−1463.
(5) Zahr, O. K.; Blum, A. S. *Nano Lett.* **2011**, *12*, 629−633.
(6) Li, F.; Gao, D.; Zhai, X.; Chen, Y.; Fu, T.; Wu, D.; Zhang, Z.-P.; Zhang, X.-E.; Wang, Q. *Angew. Chem., Int. Ed.* **2011**, *50*, 4202−4205.
(7) Pinheiro, A. V.; Han, D.; Shih, W. M.; Yan, H. *Nat. Nanotechnol.* **2011**, *6*, 763−772.
(8) Chhabra, R.; Sharma, J.; Wang, H.; Zou, S.; Lin, S.; Yan, H.; Lindsay, S.; Liu, Y. *Nanotechnology* **2009**, *20*, 485201.
(9) Pal, S.; Deng, Z.; Wang, H.; Zou, S.; Liu, Y.; Yan, H. *J. Am. Chem. Soc.* **2011**, *133*, 17606−17609.
(10) Ming, T.; Chen, H.; Jiang, R.; Li, Q.; Wang, J. *J. Phys. Chem. Lett.* **2011**, *3*, 191−202.
(11) Lakowicz, J. R. *Anal. Biochem.* **2001**, *298*, 1−24.
(12) Aslan, K.; Lakowicz, J. R.; Geddes, C. D. *Curr. Opin. Chem. Biol.* **2005**, *9*, 538−544.
(13) Aslan, K.; Gryczynski, I.; Malicka, J.; Matveeva, E.; Lakowicz, J. R.; Geddes, C. D. *Curr. Opin. Biotechnol.* **2005**, *16*, 55−62.
(14) Lakowicz, J. R. *Anal. Biochem.* **2005**, *337*, 171−194.
(15) Zhang, Y.; Aslan, K.; Previte, M. J. R.; Geddes, C. D. *Appl. Phys. Lett.* **2007**, *90*, 173116−173116−3.
(16) Wang, J.; Moore, J.; Laulhe, S.; Nantz, M.; Achilefu, S.; Kang, K. A. *Nanotechnology* **2012**, *23*, 095501.
(17) Kang, K. A.; Wang, J.; Jasinski, J. B.; Achilefu, S. *J. Nanobiotechnol.* **2011**, *9*, 16.
(18) Kühn, S.; Håkanson, U.; Rogobete, L.; Sandoghdar, V. *Phys. Rev. Lett.* **2006**, *97*, 017402.
(19) Tovmachenko, O. G.; Graf, C.; van den Heuvel, D. J.; van Blaaderen, A.; Gerritsen, H. C. *Adv. Mater.* **2006**, *18*, 91−95.
(20) Fu, Y.; Zhang, J.; Lakowicz, J. R. *J. Fluoresc.* **2007**, *17*, 811−816.
(21) Ray, K.; Zhang, J.; Lakowicz, J. R. *Anal. Chem.* **2008**, *80*, 7313−7318.
(22) Tam, F.; Goodrich, G. P.; Johnson, B. R.; Halas, N. J. *Nano Lett.* **2007**, *7*, 496−501.
(23) Bardhan, R.; Grady, N. K.; Cole, J. R.; Joshi, A.; Halas, N. J. *ACS Nano* **2009**, *3*, 744−752.
(24) Fu, Y.; Zhang, J.; Lakowicz, J. R. *J. Am. Chem. Soc.* **2010**, *132*, 5540−5541.
(25) Chen, Y.; Munechika, K.; Ginger, D. S. *Nano Lett.* **2007**, *7*, 690−696.
(26) Anger, P.; Bharadwaj, P.; Novotny, L. *Phys. Rev. Lett.* **2006**, *96*, 113002.
(27) Schneider, G.; Decher, G.; Nerambourg, N.; Praho, R.; Werts, M. H. V.; Blanchard-Desce, M. *Nano Lett.* **2006**, *6*, 530−536.
(28) Dulkeith, E.; Ringler, M.; Klar, T. A.; Feldmann, J.; Muñoz Javier, A.; Parak, W. J. *Nano Lett.* **2005**, *5*, 585−589.
(29) Acuna, G. P.; Bucher, M.; Stein, I. H.; Steinhauer, C.; Kuzyk, A.; Holzmeister, P.; Schreiber, R.; Moroz, A.; Stefani, F. D.; Liedl, T.; Simmel, F. C.; Tinnefeld, P. *ACS Nano* **2012**, *6*, 3189−3195.
(30) Singh, M. P.; Strouse, G. F. *J. Am. Chem. Soc.* **2010**, *132*, 9383−9391.
(31) Dulkeith, E.; Morteani, A. C.; Niedereichholz, T.; Klar, T. A.; Feldmann, J.; Levi, S. A.; van Veggel, F. C. J. M.; Reinhoudt, D. N.; Mller, M.; Gittins, D. I. *Phys. Rev. Lett.* **2002**, *89*, 203002.
(32) Persson, B. N. J.; Lang, N. D. *Phys. Rev. B* **1982**, *26*, 5409−5415.
(33) Yun, C. S.; Javier, A.; Jennings, T.; Fischer, M.; Hira, S.; Peterson, S.; Hopkins, B.; Reich, N. O.; Strouse, G. F. *J. Am. Chem. Soc.* **2005**, *127*, 3115−3119.
(34) Jennings, T. L.; Singh, M. P.; Strouse, G. F. *J. Am. Chem. Soc.* **2006**, *128*, 5462−5467.
(35) Härtling, T.; Reichenbach, P.; Eng, L. M. *Opt. Express* **2007**, *15*, 12806−12817.
(36) Maiti, S.; Dutta, S.; Das, P. K. *Chem.—Eur. J.* **2011**, *17*, 7538−7548.
(37) Iosin, M.; Baldeck, P.; Astilean, S. *Nucl. Instrum. Methods Phys. Res., Sect. B* **2009**, *267*, 403−405.
(38) Valegård, K.; Liljas, L.; Fridborg, K.; Unge, T. *Nature* **1990**, *345*, 36−41.
(39) Hooker, J. M.; Kovacs, E. W.; Francis, M. B. *J. Am. Chem. Soc.* **2004**, *126*, 3718−3719.
(40) Wu, W.; Hsiao, S.; Carrico, Z.; Francis, M. *Angew. Chem., Int. Ed.* **2009**, *48*, 9493−9497.
(41) Garimella, P. D.; Datta, A.; Romanini, D. W.; Raymond, K. N.; Francis, M. B. *J. Am. Chem. Soc.* **2011**, *133*, 14704−14709.

(42) Anderson, E. A.; Isaacman, S.; Peabody, D. S.; Wang, E. Y.; Canary, J. W.; Kirshenbaum, K. *Nano Lett.* **2006**, *6*, 1160−1164.
(43) Hooker, J. M.; O'Neil, J. P.; Romanini, D. W.; Taylor, S. E.; Francis, M. B. *Mol. Imaging Biol.* **2008**, *10*, 182−191.
(44) Kovacs, E. W.; Hooker, J. M.; Romanini, D. W.; Holder, P. G.; Berry, K. E.; Francis, M. B. *Bioconjugate Chem.* **2007**, *18*, 1140−1147.
(45) Tong, G. J.; Hsiao, S. C.; Carrico, Z. M.; Francis, M. B. *J. Am. Chem. Soc.* **2009**, *131*, 11174−11178.
(46) Seim, K. L.; Obermeyer, A. C.; Francis, M. B. *J. Am. Chem. Soc.* **2011**, *133*, 16970−16976.
(47) Carrico, Z. M.; Romanini, D. W.; Mehl, R. A.; Francis, M. B. *Chem. Commun.* **2008**, 1205−1207.
(48) Behrens, C. R.; Hooker, J. M.; Obermeyer, A. C.; Romanini, D. W.; Katz, E. M.; Francis, M. B. *J. Am. Chem. Soc.* **2011**, *133*, 16398−16401.
(49) Chackerian, B.; Caldeira, J.; Peabody, J.; Peabody, D. S. *J. Mol. Biol.* **2011**, *409*, 225−237.
(50) Stephanopoulos, N.; Liu, M.; Tong, G. J.; Li, Z.; Liu, Y.; Yan, H.; Francis, M. B. *Nano Lett.* **2010**, *10*, 2714−2720.
(51) Loo, L.; Guenther, R. H.; Lommel, S. A.; Franzen, S. *J. Am. Chem. Soc.* **2007**, *129*, 11111−11117.
(52) Dragnea, B.; Chen, C.; Kwak, E.-S.; Stein, B.; Kao, C. C. *J. Am. Chem. Soc.* **2003**, *125*, 6374−6375.
(53) Chen, C.; Kwak, E.-S.; Stein, B.; Kao, C. C.; Dragnea, B. *J. Nanosci. Nanotechnol.* **2005**, *5*, 2029−2033.
(54) Loo, L.; Guenther, R. H.; Basnayake, V. R.; Lommel, S. A.; Franzen, S. *J. Am. Chem. Soc.* **2006**, *128*, 4502−4503.
(55) Chen, C.; Daniel, M.-C.; Quinkert, Z. T.; De, M.; Stein, B.; Bowman, V. D.; Chipman, P. R.; Rotello, V. M.; Kao, C. C.; Dragnea, B. *Nano Lett.* **2006**, *6*, 611−615.
(56) Aniagyei, S. E.; Kennedy, C. J.; Stein, B.; Willits, D. A.; Douglas, T.; Young, M. J.; De, M.; Rotello, V. M.; Srisathiyanarayanan, D.; Kao, C. C.; Dragnea, B. *Nano Lett.* **2009**, *9*, 393−398.
(57) Daniel, M.-C.; Tsvetkova, I. B.; Quinkert, Z. T.; Murali, A.; De, M.; Rotello, V. M.; Kao, C. C.; Dragnea, B. *ACS Nano* **2010**, *4*, 3853−3860.
(58) Young, M.; Debbie, W.; Uchida, M.; Douglas, T. *Annu. Rev. Phytopathol.* **2008**, *46*, 361−384.
(59) Wu, M.; Brown, W. L.; Stockley, P. G. *Bioconjugate Chem.* **1995**, *6*, 587−595.
(60) Ashley, C. E.; Carnes, E. C.; Phillips, G. K.; Durfee, P. N.; Buley, M. D.; Lino, C. A.; Padilla, D. P.; Phillips, B.; Carter, M. B.; Willman, C. L.; Brinker, C. J.; Caldeira, J.; do, C.; Chackerian, B.; Wharton, W.; Peabody, D. S. *ACS Nano* **2011**, *5*, 5729−5745.
(61) Glasgow, J. E.; Capehart, S. L.; Francis, M. B.; Tullman-Ercek, D. *ACS Nano* **2012**, *6*, 8658−8664.
(62) Sun, J.; DuFort, C.; Daniel, M.; Murali, A.; Chen, C.; Gopinath, K.; Stein, B.; De, M.; Rotello, V.; Holzenburg, A.; Kao, C.; Dragnea, B. *Proc. Natl. Acad. Sci. U.S.A.* **2007**, *104*, 1354−1359.
(63) Mehl, R. A.; Anderson, J. C.; Santoro, S. W.; Wang, L.; Martin, A. B.; King, D. S.; Horn, D. M.; Schultz, P. G. *J. Am. Chem. Soc.* **2003**, *125*, 935−939.
(64) Hooker, J. M.; Esser-Kahn, A. P.; Francis, M. B. *J. Am. Chem. Soc.* **2006**, *128*, 15558−15559.
(65) Tinland, B.; Pluen, A.; Sturm, J.; Weill, G. *Macromolecules* **1997**, *30*, 5763−5765.
(66) Zheng, D.; Seferos, D.; Giljohann, D.; Patel, P.; Mirkin, C. *Nano Lett.* **2009**, *9*, 3258−3261.